European Journal of Pharmaceutical Sciences 212 (2025) 107182

Contents lists available at ScienceDirect

European Journal of Pharmaceutical Sciences

journal homepage: www.elsevier.com/locate/ejps

The impact of lipid compositions on siRNA and mRNA lipid nanoparticle performance for pulmonary delivery

Stina Rademacker [a], Simone Pinto Carneiro [a], Müge Molbay [a], Federica Catapano [a], Ignasi Forné [b], Axel Imhof [b], Richard Wibel [c], Christoph Heidecke [c], Peter Hölig [c], Olivia M. Merkel [a,d,e,*]

[a] Department of Pharmacy, Ludwig-Maximilians-Universität München, Butenandtstrasse 5-13, 81377 Munich, Germany
[b] Proteomics Core Facility, BioMedical Center, Faculty of Medicine, Ludwig-Maximilians-Universität München, Großhadernerstr. 9, 82152 Planegg-Martinsried, Germany
[c] Lipoid GmbH, Frigenstr. 4, 67065 Ludwigshafen, Germany
[d] Center for NanoScience (CeNS), Ludwig-Maximilians-Universität München, 80799 Munich, Germany
[e] Ludwig-Maximilians-Universität München, Member of the German Center for Lung Research (DZL), Germany

ARTICLE INFO

Keywords:
RNA delivery
LNP
Phospholipids
Pulmonary delivery
Protein corona

ABSTRACT

Lipid nanoparticles (LNPs) are of significant interest as delivery systems for various RNA therapeutics, not least due to their outstanding success in applications including the COVID-19 vaccines and the siRNA therapeutic Onpattro®. As LNPs consist of different lipids, the lipid composition determines key properties of these particles. This study examines how lipid composition, especially helper and PEG-lipids, and RNA cargo (siRNA and mRNA) affect LNP performance in pulmonary delivery. By comparing two different helper and two different PEG-lipids, we assessed the impact on fusogenicity and endosomal escape, *in vitro* transfection efficiency, and subsequently protein corona formation. Their *in vitro* performance was assessed in the air-liquid interface (ALI) cell culture model, a sophisticated *in vitro* model of the lungs. Our results demonstrated that transfection efficiency and stability differ between the helper lipids DOPE and DSPC, depending on the RNA cargo. These differences can be attributed to the structural differences of the lipids and the different properties of the RNA molecules. Our investigations further demonstrated successful mucus penetration of all LNPs and 24–42 % gene silencing *in vitro*. We also explored mucus proteins/LNP interactions in human lung mucus, finding distinct protein corona formation for DSPC- and DOPE-containing LNPs. This comprehensive analysis highlights the critical role of helper lipids in combination with RNA cargo in determining LNP properties, efficiency, and *in vitro* performance, providing valuable insights for optimizing RNA delivery systems.

1. Introduction

Over the past few years, lipid nanoparticles (LNPs) have established themselves as a delivery system for various types of RNA. The FDA approval of Onpattro®, the first small interfering RNA (siRNA)-based drug, followed by the mRNA vaccines from BioNTech/Pfizer and Moderna, has paved a promising path for the application of these RNA therapeutics utilizing LNPs as a delivery platform (Akinc et al., 2019; Schoenmaker et al., 2021). LNPs function for both cargos as delivery systems, although the structural properties, such as length, charge density, and stability differ significantly between siRNA and mRNA. mRNA is single-stranded and typically consists of >1000 bases, making it relatively large and complex in structure. In contrast, siRNA is double-stranded and consists of only about 21 base pairs, making its structure comparatively small, less bulky, and less complex but rigid (Yin et al., 2014). Whereas siRNA can be used to selectively silence specific genes, mRNA enables the expression of desired proteins within cells. Both approaches have significant therapeutic relevance. Exploiting these two mechanisms enables the treatment of numerous diseases associated with increased or decreased protein expression (Yin et al., 2014). A substantial proportion of currently untreatable diseases are represented by respiratory diseases. In 2017, chronic respiratory diseases were responsible for 3.9 million deaths globally (Labaki and Han, 2020). The application of RNA-based therapies in this context shows great promise. Delivery of RNA via LNPs for direct administration to the lungs is an ideal approach for treating respiratory diseases. Pulmonary

* Corresponding author.
E-mail address: olivia.merkel@lmu.de (O.M. Merkel).

https://doi.org/10.1016/j.ejps.2025.107182
Received 28 March 2025; Received in revised form 18 June 2025; Accepted 23 June 2025
Available online 24 June 2025

Table 1
Lipid composition of LNP formulations LNP1 - LNP4 for both siRNA and mRNA LNPs.

MOLAR RATIO [%MOL]	LNP 1	LNP 2	LNP 3	LNP 4
50	Dlin-MC3-DMA	Dlin-MC3-DMA	Dlin-MC3-DMA	Dlin-MC3-DMA
38.5	Cholesterol	Cholesterol	Cholesterol	Cholesterol
10	DOPE	DOPE	DSPC	DSPC
1.5	PEG-DMG	PEG-DMPE	PEG-DMG	PEG-DMPE

delivery offers numerous advantages, including non-invasiveness, localized delivery resulting in reduced dosage and side effects, a large alveolar surface area, and minimal nuclease activity (Shaffer, 2020; Kandil and Merkel, 2019). However, pulmonary delivery also presents challenges for LNPs as a delivery system. One of the biggest hurdles that LNPs must overcome to reach the target cells is the mucus layer covering the pulmonary epithelium and the mucociliary clearance (Tafech et al., 2024).

To address the challenges associated with pulmonary delivery, this study evaluated the impact of variations in helper lipids, PEG-lipids, and RNA cargo on the physicochemical properties and *in vitro* performance of LNPs. LNPs typically consist of four different lipid components: an ionizable lipid, a cholesterol (derivative), a helper lipid, which is often a phospholipid, and a PEG-lipid (Hald Albertsen et al., 2022). For our study, we based our formulations on the established Onpattro® composition. The LNP formulations consistently contained the ionizable lipid Dlin-MC3-DMA (MC3), essential for encapsulating RNA, and cholesterol, which is crucial for the structure and stability of the LNPs (Hald Albertsen et al., 2022). Additionally, the formulations incorporated one of two different helper lipids, namely 1,2-dioleoyl-*sn*-glycero-3-phosphoethanolamine (DOPE) or 1,2-distearoyl-*sn*-glycero-3-phosphocholine (DSPC), and one of two PEG-lipids, namely 1,2-dimyristoyl-*rac*-glycero-3-[methoxy(polyethylene glycol)-2000] (PEG-DMG) or 1,2-dimyristoyl-*sn*-glycero-3-phosphoethanolamine-*N*-[methoxy(polyethylene glycol)-2000] (PEG-DMPE). Helper lipids play a vital role within LNPs, significantly contributing to their overall structure, stability, and functionality (Kulkarni et al., 2019). As demonstrated by Kauffmann et al., they can also have an impact on transfection efficiency (Kauffman et al., 2015). Due to their diverse chemical structures, different helper lipids can influence interactions with cellular membranes, such as the endosomal membrane, substantially affecting cytosolic release of RNA and, therefore, transfection efficiency (Kulkarni et al., 2017). Helper lipids are also important in protein corona formation, potentially influencing biodistribution, cellular uptake, and targeting (Zhang et al., 2021). PEG-lipids are primarily responsible for LNP colloidal stability. By forming the outer shell of the LNPs with the acyl chain anchored in the LNP and the hydrophilic PEG chain sticking out, they prevent aggregation or coalescence of the LNPs (Suzuki et al., 2020). While this is one of the most important roles of PEG-lipids, they can also influence other LNP properties, such as immunogenicity by shielding the particles from opsonization and affecting the formation of the protein corona, which in turn influences *in vivo* distribution (Knop et al., 2010).

As discussed above, key properties of LNPs that contribute to transfection efficiency are influenced by their lipid compositions. To further investigate this observation, we first evaluated the physicochemical properties of various LNP lipid compositions containing siRNA or mRNA. Next, we compared the performance of these formulations in terms of cellular uptake, gene silencing or expression efficiencies, respectively, using a submerged cell culture model. As extensively reported in the literature, most RNA-based LNPs taken up by the cells remain trapped in the endosome, limiting their biological activity. To better understand how different lipids influence this process, we also assessed their endosomal escape ability. Since submerged models have limitations in replicating the complexity of lung barriers and the pulmonary environment, we further investigated LNP performance using an air-liquid interface (ALI) model. Cells cultured at the ALI form a pseudostratified epithelium, allowing for their differentiation into a mucociliary phenotype with mucus production and tight-junction formation (Baldassi et al., 2022). These characteristics better represent lung conditions, providing a more realistic model to assess the capacity of the LNPs to overcome key lung barriers such as mucus. Additionally, we investigated the formation of the protein corona on LNPs with regards to pulmonary delivery and their lipid composition. This was accomplished by analyzing the adsorption of proteins from lung mucus onto the surface of the LNPs.

2. Materials and methods

2.1. LNP preparation

The siRNA-loaded and mRNA-loaded LNP formulations were based on the clinically approved Onpattro® formulation. In total, six lipids were employed in this study: (6Z,9Z,28Z,31Z)-heptatriaconta-6,9,28,31-tetraen-19-yl 4-(dimethylamino)butanoate (Dlin-MC3-DMA (MC3), MedChemExpress, Monmouth Junction, USA) as ionizable lipid, cholesterol (Sigma Aldrich, Taufkirchen, Germany), as helper lipids either 1,2-distearoyl-*sn*-glycero-3-phosphocholine (DSPC, Sigma Aldrich, Taufkirchen, Germany) or 1,2-dioleoyl-*sn*-glycero-3-phosphoethanolamine (DOPE, Lipoid GmbH, Ludwigshafen, Germany) and as PEGylated lipid either 1,2-dimyristoyl-*rac*-glycero-3-[methoxy(polyethylene glycol)-2000] (PEG-DMG 2000, Lipoid GmbH, Ludwigshafen, Germany) or 1,2-dimyristoyl-*sn*-glycero-3-phosphoethanolamine-*N*-[methoxy(polyethylene glycol)-2000] (PEG-DMPE, Lipoid GmbH, Ludwigshafen, Germany). RNA cargos that were encapsulated in this study were siRNA against the green fluorescent protein (GFP) gene (siGFP) and a scrambled negative control siRNA (siNC), both of which were obtained from Merck (Darmstadt, Germany). siRNA targeting human GAPDH (siGAPDH) was purchased from Integrated DNA Technologies (Leuven, Belgium), and mRNA encoding for eGFP (mGFP) was purchased from RiboPro (Oss, The Netherlands).

Four siRNA and four mRNA-LNP formulations were prepared following the composition described in Table 1. The lipids were separately dissolved in absolute ethanol and blended following the molar ratios of 50:38.5:10:1.5 mol % (Dlin-MC3-DMA, cholesterol, the corresponding helper lipid, and PEG-lipid, respectively). The lipid blends were diluted to either 2 mM for siRNA or 1 mM for mRNA. RNA was diluted in 25 mM sodium acetate buffer at pH 4.0 to achieve a nitrogen-to-phosphate (N/P) ratio of 3 for siRNA or 6 for mRNA.

The RNA-loaded LNPs were prepared using either pipette mixing or microfluidic methods. For pipette mixing, the lipid blend was directly mixed into the RNA solution by pipetting it rapidly up and down. The resulting mixture was incubated for 15 min at room temperature, followed by the addition of PBS pH 7.4 for pH increase. The microfluidic method for LNP production was carried out using the staggered herringbone mixing microfluidic chip (Fluidic 187, Microfluidic Chip-Shop, Jena, Germany). The lipid blend and the RNA dilution were mixed at a ratio of 3:1 (v/v RNA:lipids) and a total flow rate (TFR) of 3 mL/min. Buffer exchange and pH adjustment were subsequently performed by overnight dialysis at 4 °C against PBS (pH 7.4) using the Pur-A-Lyzer™ Maxi Dialysis kit (3.5 kDa molecular weight cutoff, Sigma Aldrich, Taufkirchen, Germany). After preparation, the LNP formulations were sterile filtered with a 0.22 µm Acrodisc® syringe filter (Pall, Dreieich, Germany) and stored at 4 °C until further use.

2.2. Physicochemical characterization of RNA-loaded LNPs

The LNP formulations produced via microfluidics were analyzed regarding their hydrodynamic diameter, polydispersity index (PDI), and zeta potential using the Zetasizer Advance Ultra (Malvern Instruments, Malvern, UK). For the determination of the hydrodynamic diameter and

PDI, dynamic light scattering (DLS) with a backscatter angle detection at 173° was used. The samples were directly added to disposable plastic micro cuvettes and the measurements were carried out at 25 °C. The zeta potential was assessed via Phase Analysis Light Scattering (PALS) by diluting the samples 1:7 with PBS and using a folded capillary zeta cell (DTS1070, Malvern Instruments, Malvern, UK). Samples were measured in triplicate ($n = 3$) and the resulting data was analyzed with the ZS Xplorer software (v.3.20).

2.3. Encapsulation efficiency and RNA binding capacity

The efficiency of the encapsulation of the RNA cargo in LNPs prepared manually and via microfluidics was assessed via RiboGreen™ assay. Either 5 µL of TE buffer (Sigma Aldrich, Taufkirchen, Germany) or 5 µL of a 2 % Triton-X 100 solution in TE buffer (Sigma Aldrich, Taufkirchen, Germany) were added to a black, flat bottom 384-well plate, followed by 5 µL of LNP sample or RNA standard samples in triplicate. For the RNA standard curve, a serial dilution ranging from 10 ng/µL to 0.625 ng/µL in TE buffer was prepared. The plate was incubated for 60 min at 37 °C in a shaking incubator. Subsequently, 10 µL of Quant-iT™ RiboGreen™ solution (Invitrogen™, Thermo Fisher Scientific, Schwerte, Germany), diluted 1:100 in TE buffer, was added to each well. The readout was performed after 10 min of incubation using a microplate reader (Tecan Spark, TECAN, Männedorf, Switzerland) with an excitation wavelength of 488 nm and an emission wavelength of 525 nm. To assess the percentage of RNA binding, the same method was used, but without the addition of Triton-X, allowing for the quantification of free and unbound RNA within the LNPs, respectively (Carneiro et al., 2024).

2.4. Morphological characterization of LNPs via cryogenic transmission electron microscopy (CryoTEM)

For CryoTEM imaging, 3.5 µL of siRNA-containing LNPs, produced via microfluidics, were applied to 2 nm pre-coated Quantifoil R3/3 holey carbon-supported grids and either vitrified using Vitrobot Mark IV (FEI/Thermo Fisher) or negatively stained using 2 % uranyl acetate. Negatively stained grids were analyzed using a Megaview 1024 × 1024 pixel CCD camera (iTEM) at different magnifications on a Morgagni TEM (FEI/ThermoFisher) at 100 kV. Images of vitrified samples were collected under low dose conditions at various nominal magnifications using EM-TOOLS (TVIPS GmbH) on a Tecnai G2 Spirit transmission electron microscope (FEI/ThermoFisher) equipped with a F218 2048 × 2048 pixel CCD camera (TVIPS GmbH) at 120 kV.

2.5. Cell culture

For *in vitro* assessment of gene silencing efficiency in submerged cell culture, the human non-small cell lung carcinoma cell line (H1299/GFP) expressing the enhanced green fluorescent protein (eGFP) as a reporter gene was employed. The cells were cultured in 75 cm^2 flasks using RPMI-1640 medium supplemented with 10 % fetal bovine serum (FBS, Sigma Aldrich, Taufkirchen, Germany), 1 % penicillin/streptomycin (P/S, Thermo Fisher Scientific, Darmstadt, Germany), and 0.4 % G418 disulfate salt solution (Sigma Aldrich, Darmstadt, Germany). For cellular uptake and endosomal escape evaluation, the human non-small cell lung carcinoma cell line H1299 was used and cultured in RPMI-1640 with 10 % FBS and 1 % P/S.

The human lung adenocarcinoma cell line Calu-3 was purchased from ATCC (HTB-55, Manassas, VA, USA) and cultured in EMEM supplemented with 10 % FBS. To establish an ALI cell culture (Fig. 2), the cells were seeded at a density of 250,000 cells in 100 µL of medium onto uncoated Transwell® polyester membrane cell culture inserts (6.5 mm, 0.4 µm pore size) (Corning, New York, USA). Additionally, 700 µL of EMEM was added to the basolateral chamber of the 24 well plate holding the Transwells®. After three days, the airlift was performed by removing the medium from the apical side. Subsequently, the Transwells® were then moved into new wells containing 200 µL of PneumaCult™ ALI medium (STEMcell technology, Vancouver, Canada). The ALI medium was exchanged every two days. Transepithelial electrical resistance (TEER) measurements were conducted with the EVOM epithelial volt/ohm meter (World Precision Instruments, Sarasota, USA). Transfections with LNPs prepared via microfluidics were performed one week after the air-lift, when TEER values above 300 Ω*cm^2 were reached. All cells were maintained in a humidified atmosphere at 37 °C and 5 % CO_2. Cell passaging and seeding were performed at about 80 % confluency.

2.6. Cellular uptake of siRNA-loaded LNPs in submerged cell culture

H1299 cells were seeded at a density of 25,000 cells/well in a 24-well plate. After 24 h of incubation at 37 °C and 5 % CO_2, the cells were transfected with 100 pmol siRNA-loaded LNPs, prepared via microfluidics, consisting of 10 % AF488-labeled siRNA and 90 % negative control siRNA (siNC), and incubated for 24 h at 37 °C and 5 % CO_2. PBS was used as a blank control, and for the positive control, the same siRNA dose was combined with Lipofectamine 2000 (Thermo Fisher Scientific, Darmstadt, Germany) according to the manufacturer's protocol. Following the incubation, the cells were washed once with PBS and then incubated for 5 min with 100 µL of trypsin 0.05 % (Thermo Fisher Scientific, Darmstadt, Germany) at 37 °C and 5 % CO_2 for detachment. After adding 100 µL of 10 % FBS-containing medium, the cells were centrifuged for 5 min at 400 x g, washed twice with PBS, and resuspended in PBS supplemented with 2 mmol EDTA (Sigma Aldrich, Taufkirchen, Germany). To assess the cellular uptake, the mean fluorescence intensity (MFI) was measured in triplicate ($N = 3$) using flow cytometry (Attune Nxt instrument, Thermo Fisher Scientific, Darmstadt, Germany). The gating was adjusted to ensure analysis of at least 10,000 viable cells. Measurements were conducted with an excitation wavelength of 488 nm and a 530/30 nm bandpass emission filter.

2.7. Gene silencing efficiency of siRNA-loaded LNPs in submerged cell culture

H1299/eGFP cells were used to assess the gene silencing efficiency of siRNA LNPs produced via microfluidics. The cells were seeded at a density of 25,000 cells per well 24 h prior to transfection with LNPs encapsulating siGFP. As a positive control, Lipofectamine 2000 mixed with siGFP was used, and free siGFP was used as a negative control. After 24 h of incubation, cells were trypsinized, washed with PBS, centrifuged, and resuspended in PBS containing 2 mmol EDTA. The cell suspension was analyzed via flow cytometry, assessing the MFI of at least 10,000 viable cells per sample with an excitation at 488 nm and a 530/30 nm bandpass emission filter.

2.8. mRNA expression in submerged cell culture

To assess the mRNA expression efficiency in submerged cell culture, H1299 cells were seeded at a density of 25,000 cells per well in a 24-well plate. After 24 h the cells were transfected with 100 ng of mRNA encoding for eGFP (mGFP) encapsulated into the four mRNA LNP formulations, which were prepared via microfluidics. Following a 24 h incubation time, cells were trypsinized, washed with PBS, centrifuged, and resuspended in PBS containing 2 mmol EDTA. The cell suspension was analyzed via flow cytometry, assessing the MFI of at least 10,000 viable cells with an excitation at 488 nm and a 530/30 nm bandpass emission filter.

2.9. Endosomal escape of siRNA-loaded LNPs in submerged cell culture

The ability of the siRNA-loaded LNPs to escape the endosome was assessed in H1299 cells. The cells were seeded at a density of 10,000 cells per well on a chambered coverslip (µ-Slide 8 Well, ibidi, Gräfelfing, Germany) 24 h prior to transfection with LNPs produced via

microfluidics and encapsulating 20 pmol AlexaFluor647-labeled siRNA. After 24 h of incubation, 2 µL of 10 µM Lysotracker™ green solution (Thermo Fisher Scientific, Darmstadt, Germany) were added to the wells for 1 h and washed off with PBS. Cells were fixed with 4 % paraformaldehyde solution for 15 min at 4 °C and washed three times with PBS. Subsequently, nuclei were stained with 1 µg/mL 4′,6-diamidino-2-phenylindole solution (DAPI, Thermo Fisher Scientific, Darmstadt, Germany) for 15 min and washed twice with PBS. The cells were analyzed using a SP8 inverted confocal microscope (Leica Camera, Wetzlar, Germany). The confocal images were processed using the software ImageJ with the plugin JACoP to assess the Pearson's correlation coefficient.

2.10. Assessment of efficiency in submerged cell culture after storage of siRNA-loaded LNPs

To evaluate the stability of the siRNA-loaded LNP formulations, LNP1 – 4 were prepared via microfluidics and stored at 4 °C (F), and 25 °C (RT) for 10 weeks. At predetermined time-points (T0 (freshly prepared LNPs), T1 (1 week), T2 (6 weeks), and T3 (10 weeks)), gene knockdown efficiency, particle size and PDI were analyzed. In addition, at T0 and T3 the siRNA loss or leakage was investigated. Cell transfection and gene silencing efficiency experiments in H1299 eGFP cells were conducted as described in 2.7, particle size and PDI were measured as described in 2.2. For the quantification of the siRNA loss, the method described in 2.3 was used without the addition of Triton-X, focusing solely on the quantification of free, unencapsulated siRNA.

2.11. Cellular uptake of siRNA-loaded LNPs in Calu-3 cells cultured at the air-liquid interface

To evaluate the pulmonary uptake efficiency of siRNA-loaded LNPs, Calu-3 cells cultured at the air-liquid interface were used. The cells were prepared as described in section 2.5. One week after the airlift was performed, cells were transfected with LNPs prepared via microfluidics and which were loaded with AlexaFluor488 (AF488)-labeled siRNA (100 pmol per well, 10 % labeled siRNA). After 24 h the cells were washed twice with PBS and collected in an Eppendorf tube by gently scraping them off the membrane using a pipette tip. Prior to the readout via flow cytometry (Attune Nxt instrument, Thermo Fisher Scientific, Darmstadt, Germany), the cells were centrifuged for 5 min at 400 x g and washed twice with PBS. The cell pellet was resuspended in PBS containing 2 mmol EDTA (Sigma Aldrich, Taufkirchen, Germany). To evaluate the uptake of the labeled siRNA, the MFI was recorded using an excitation at 488 nm and a 530/30 nm bandpass emission filter.

2.12. In vitro GAPDH gene knockdown of siRNA-loaded LNPs in Calu-3 cells cultured at the air-liquid interface

Gene knockdown efficiency of siRNA LNPs was evaluated in cells cultured at the ALI as a physiologically relevant model. Calu-3 cells were prepared as described in section 2.5 and transfected with each of the four LNP formulations prepared via microfluidics and encapsulating 150 pmol of siRNA against GAPDH (siGAPDH). As control, Onpattro®-like LNPs encapsulating 150 pmol of negative control siRNA (siNC) were used. Cell harvesting was performed 48 h after transfection by washing them twice with PBS and gently scraping the cells off the membrane. RNA was isolated from the cell suspension using the PureLink RNA mini kit (Thermo Fisher Scientific, Darmstadt, Germany), following the manufacturer's instructions with additional DNase digestion. Subsequently, cDNA synthesis was conducted with the high-capacity cDNA synthesis kit (Thermo Fisher Scientific, Darmstadt, Germany). Finally, qPCR was run using the QuantStudio 3 Real-Time PCR System (Thermo Fisher Scientific, Darmstadt, Germany), SYBR™ Green PCR Master Mix (Thermo Fisher Scientific, Darmstadt, Germany), and primers for human GAPDH (Qiagen, Hilden Germany) and β-actin (Qiagen, Hilden, Germany) for normalization.

2.13. Cellular uptake of siRNA-loaded LNPs in Calu-3 cells cultured at the air-liquid interface

Calu-3 cells cultured at the ALI were prepared as described in 2.5. For transfection, LNP formulation LNP2 prepared via microfluidics and encapsulating 100 pmol of 10 % Cyanine 5 (Cy5)-labeled siRNA and free, labeled siRNA as a negative control were used. For imaging, nuclei were stained with 300 µL of a 1:200 dilution of 10 mg/mL Hoechst (Thermo Fisher Scientific, Schwerte, Germany) solution from the basolateral side and the mucus was stained with 100 µL of a 1:100 dilution of 1 mg/mL AlexaFluor488-labeled Wheat-Germ-Agglutinin solution (AF488-WGA, Thermo Fisher Scientific, Schwerte, Germany) from the apical side and incubated for 20 min. The confocal microscopy images were taken after washing the cells three times from the apical and basolateral side with PBS, cutting out the Transwell membrane and mounting it onto a microscope slide with one drop of FluorSave™ Reagent (Merck KGaA, Darmstadt, Germany). For imaging, a Leica SP8 inverted confocal microscope (Leica Camera, Wetzlar, Germany) with a 20-fold magnitude was used. Editing was performed with the software ImageJ.

2.14. Protein corona formation on LNPs in Calu-3-derived mucus

Calu-3 cells were cultured at the ALI to secrete mucus, which was collected after one week. siRNA-loaded LNP formulations 1–4 were prepared via microfluidics and incubated with the harvested mucus overnight at 4 °C to assess protein corona formation. The LNPs were purified using a 100 kDa molecular weight cutoff spin column (Vivaspin 6, Sigma-Aldrich), followed by resuspension to the original volume and additional washing. Protein corona-coated LNPs were then centrifuged with ice-cold 70 % acetone at 17,000 x g for 45 min. LNP samples were resuspended in 4 % SDS-Tris–HCl buffer, heated at 95 °C, sonicated, and digested overnight with Trypsin-LysC. After acidification and purification using Evotips, eluted peptides were dried and resuspended in 0.1 % trifluoroacetic acid for mass spectrometry analysis. LC-MS/MS was performed on an Orbitrap Q Exactive HF coupled with an Ultimate-3000nRSLC, using DIA mode. Data were processed and searched against the human UniProt database with DIA-NN, and differential protein expression was calculated with PG.MaxLFQ. Differentially expressed proteins (DEPs) were identified with thresholds of $P < 0.05$ and $|\log \text{fold change}| > 0.5$, and visualized via volcano plot.

2.15. Statistical analysis

All experiments were conducted in triplicates with technical replicates. The results indicate mean values ± SEM. For statistical analysis, the collected data was analyzed with GraphPad Prism (GraphPad Software, La Jolla, USA). For p-values (95% confidence interval), a one-way ANOVA was conducted using Tukey multiple comparison as post-test.

3. Results

3.1. Physicochemical characterization of siRNA and mRNA-loaded LNPs

The four LNP formulations encapsulating either siRNA or mRNA were prepared either via microfluidics or pipette mixing. Formulation LNP3 was similar to Onpattro®, while LNP4 contained PEG-DMPE instead of PEG-DMG. LNP1 contained DOPE instead of DSPC in LNP3, and in formulation LNP2, both alternatives, namely PEG-DMPE and DOPE were used (Table 1). To assess the physicochemical properties of these LNPs such as hydrodynamic diameter, zeta potential, and PDI, DLS and PALS measurements were conducted with the LNPs prepared via microfluidics. Notably, no substantial differences in size and PDI were observed among the different formulations (LNP1–4), regardless of

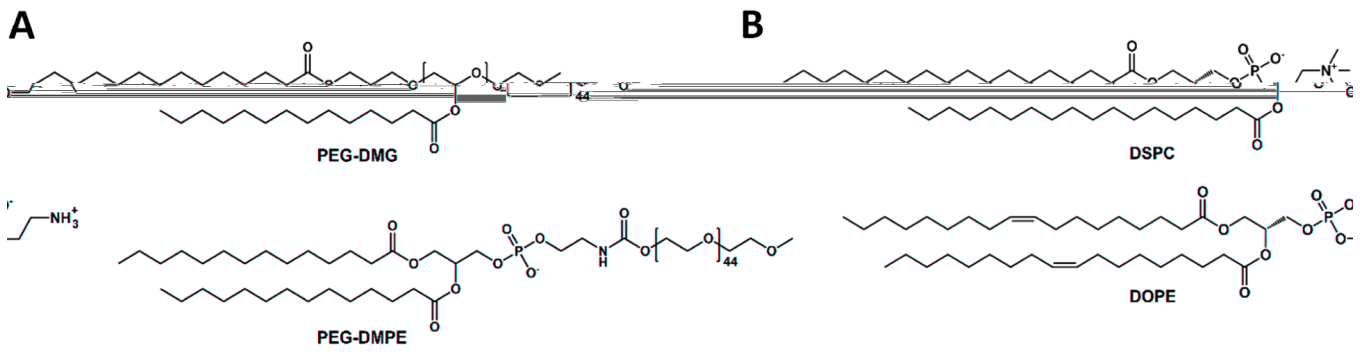

Fig. 1. Structures of the different PEG and helper lipids used in the LNP formulations in Table 1. A) PEG-DMG and PEG-DMPE, and B) the helper lipids DSPC and DOPE.

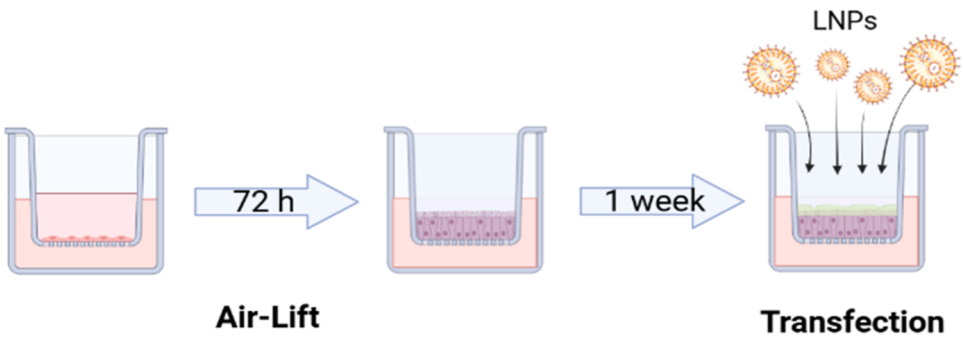

Fig. 2. Schematic representation of the experimental workflow for culturing cells at ALI conditions.

whether siRNA or mRNA was used as cargo (Fig. 3A, B). All LNP formulations exhibited suitable sizes of approximately 100 nm and narrow size distributions, as indicated by low PDI values (< 0.2). The zeta potential ranged from 1 to 10 mV (Figure S 1A, B) across the formulations, attributing an approximately neutral surface charge to the particles (Clogston and Patri, 2011). The siRNA encapsulation efficiency was around 72 %, with no significant differences among the various formulations (Figure S 1C). A similar trend was observed for mRNA-loaded LNPs, although their encapsulation efficiency was slightly higher, around 79 % (Figure S 1D). When LNPs were prepared manually via pipette mixing, the encapsulation efficiency was analyzed without the potential influence of RNA loss from additional LNP processing steps such as dialysis or filtration. In this context, different results were obtained for siRNA and mRNA. LNPs encapsulating mRNA showed no substantial changes due to different lipid compositions in the formulations (Fig. 3D). In contrast, siRNA-loaded LNPs exhibited higher siRNA encapsulation in case of formulations LNP3 and LNP4 compared to LNP1 and LNP2 (Fig. 3C). The distinction between these two groups lies in the helper lipid used: LNP3 and LNP4 contain DSPC, whereas LNP1 and LNP2 contain DOPE.

3.2. Morphological characterization of LNPs via CryoTEM

CryoTEM images revealed different morphologies of siRNA-loaded LNP2 and LNP4 (Fig. 4), which differed only in the substitution of DSPC (LNP4) with DOPE (LNP2). LNP2, containing DOPE, exhibited clearly visible hexagonal structures, indicating the existence of inverted hexagonal phases (H_{II}). Additionally, the overall LNP structure seemed less round, promoting the presence of the hexagonal structures (Fig. 4A). For LNP4 with DSPC as helper lipid, a lamellar, rounder structure was observed, with visible lipid bilayers (Fig. 4B). This is in alignment with Pattipeiluhu et al., who demonstrated that increasing the DOPE content in LNPs leads to a higher prevalence of inverted hexagonal phases (H_{II}) compared to lamellar structures, which are observed at a DOPE content of 10 % in CryoTEM images (Pattipeiluhu et al., 2024). Overall, the CryoTEM images confirmed that DOPE leads to inverted hexagonal structures within the LNPs tested, in contrast to DSPC-containing LNPs, which exhibited predominantly lamellar structures.

3.3. In vitro performance of siRNA and mRNA-loaded LNPs: cellular uptake, gene silencing, and expression efficiency

To evaluate cellular uptake, H1299 cells were transfected with labeled siRNA-loaded LNPs. As shown in Fig. 5A, the increased fluorescence values of the treated cells indicate successful uptake of all LNP formulations. Among the four formulations, LNP3 and LNP4 mediated the most efficient cellular uptake, performing comparably to or surpassing the positive control with Lipofectamine. The formulations LNP1 and LNP2 showed lower uptake, with LNP1 demonstrating the lowest uptake among all formulations. Free siRNA, due to its size and negative charge, cannot penetrate the cell membrane and is not taken up by the cells. Despite similar encapsulation efficiencies and higher cellular uptake observed for DSPC-containing formulations (LNP3 and LNP4), these LNPs demonstrated significantly lower gene silencing efficiency compared to DOPE-containing formulations (LNP1 and LNP2) in H1299/eGFP cells (Fig. 5B). LNP1 and LNP2 performed similarly to the positive control Lipofectamine. Accordingly, formulations containing the helper lipid DSPC demonstrated better cellular uptake, yet they exhibited significantly lower gene silencing efficiency compared to DOPE-containing LNPs. This effect is primarily dependent on the helper lipid, as evidenced by the clear distinction in efficiency between DOPE and non-DOPE LNPs. The alteration of PEG-lipids appeared to have little to no impact on transfection efficiency. To further determine the transfection efficiency, eGFP expression was measured in H1299 cells transfected with mGFP-loaded LNPs (Fig. 5C), using the same four formulations as in the previous experiments. Although MC3 was designed for siRNA delivery and other ionizable lipids such as the clinically approved SM102 or ALC-0315 show much higher efficiency for mRNA

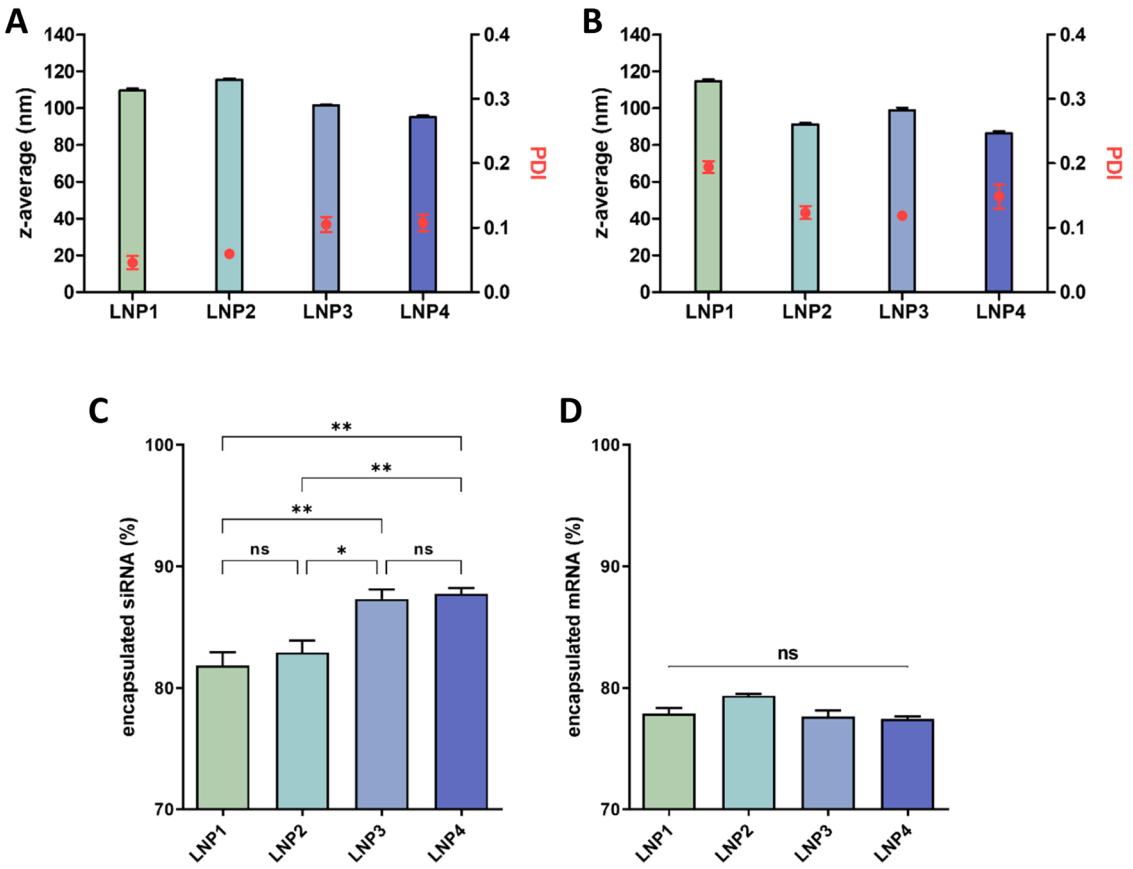

Fig. 3. Physicochemical characterization of siRNA- and mRNA-loaded LNPs. **(Panels A, B)** Hydrodynamic diameter and PDI of **A**) siRNA- and **B**) mRNA-loaded formulations LNP1–4 prepared via microfluidics in PBS at pH 7.4 as assessed using DLS. (**Panels C, D)** RNA encapsulation efficiency of manually prepared **C**) siRNA- and **D**) mRNA-loaded LNP formulations. (Values indicate mean ± SEM, $n = 3$, One-way ANOVA, *, $p < 0.05$, **, $p < 0.01$).

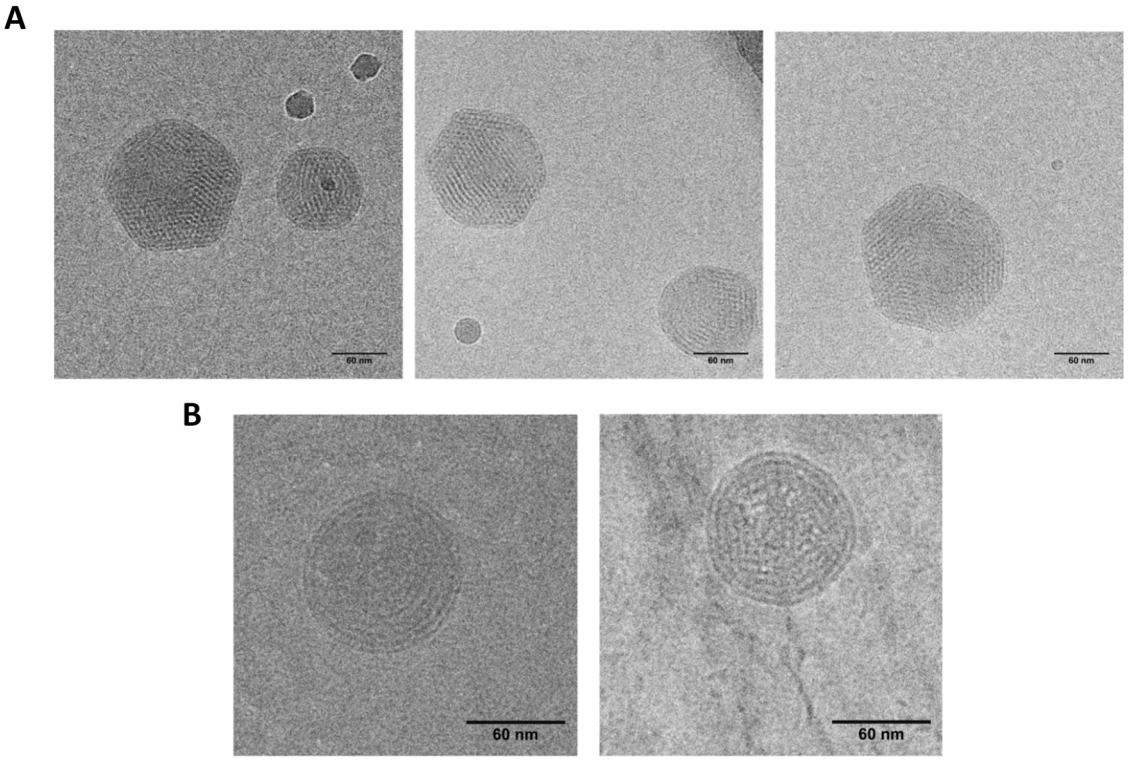

Fig. 4. CryoTEM images of siRNA-loaded LNP formulations LNP2 and LNP4 prepared via microfluidics, scale bars represent 60 nm. A) Images of representative structures of LNP2 with visible hexagonal structures. B) Images of representative structures of LNP4 showing a lamellar structure.

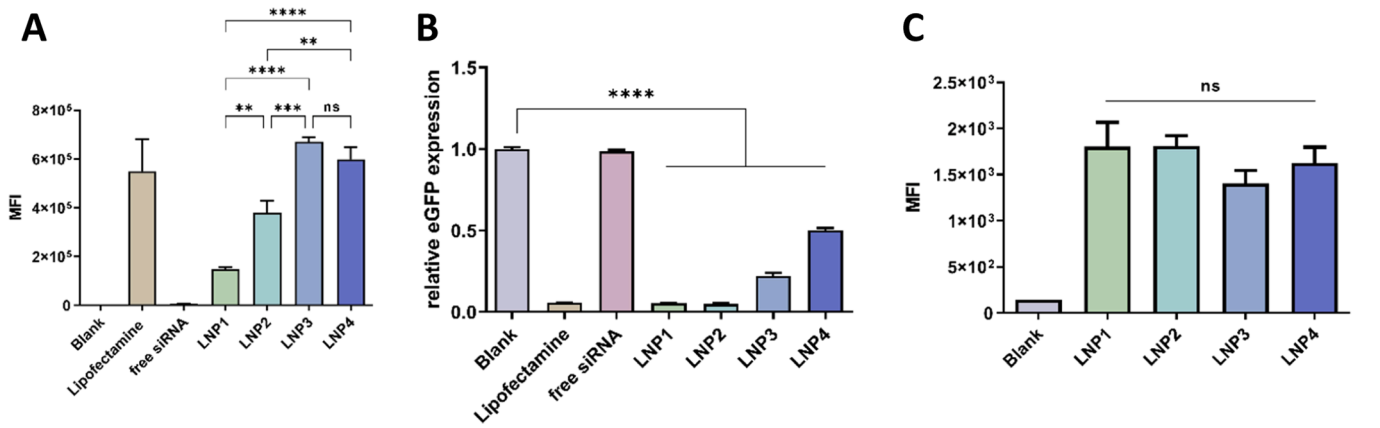

Fig. 5. *In vitro* performance of LNPs prepared via microfluidics. **A**) Cellular uptake in H1299 cells transfected with 10 pmol AF488 labeled siRNA encapsulated in either LNP1–4 or Lipofectamine 2000 as positive control. As negative control, 10 pmol free labeled siRNA was used. Blank represents untreated cells. MFI was assessed via flow cytometry. **B**) eGFP knockdown in H1299/GFP cells 48 h after transfection with 10 pmol siGFP containing LNP1–4. Blank represents untreated cells, Lipofectamine 2000 encapsulating 10 pmol siGFP as positive control, and free siGFP as negative control. eGFP expression was evaluated via flow cytometry. **C**) eGFP expression in H1299 cells transfected with 100 ng mGFP-loaded LNPs 1–4. eGFP expression was assessed as MFI 24 h after transfection using flow cytometry. (Values indicate mean ± SEM, $N = 3$, One-way ANOVA, **, $p < 0.01$, ***, $p < 0.001$, ****, $p < 0.0001$).

transfection, this approach was chosen to further investigate the properties of the lipid composition (Jayaraman et al., 2012; Escalona-Rayo et al., 2023). All formulations effectively delivered mGFP into the cells with no significant differences among the four different formulations regarding eGFP expression levels (Fig. 5C). Neither the alteration of the helper lipid nor the PEG-lipid had a significant impact.

3.4. Endosomal escape of siRNA-loaded LNPs in H1299 cells

Following cellular uptake, most siRNA molecules are trapped in the endosome, preventing them from reaching the cytosol and rendering them ineffective (Suzuki and Ishihara, 2021). Therefore, to understand key differences in transfection efficiencies of lipid formulations, assessing endosomal escape is valuable. To evaluate the role of helper lipids in promoting endosomal escape, siRNA LNP formulations 1 and 3, containing either DSPC (LNP3) or DOPE (LNP1) as helper lipid, were utilized (Fig. 6). In both cases, the AlexaFluor647-labeled siRNA was found in the perinuclear area of the cells, as depicted in red. The late endosomes in the cytoplasm were stained using Lysotracker™ (green) and the nuclei were stained with DAPI (blue) (Fig. 6A). The overlap of green and red fluorescence yields the yellow signal, which indicates colocalization of siRNA within the late endosomes, meaning the siRNA is trapped in the endosome. This colocalization was more prominently shown after transfection with LNP3. In contrast, sparse localization of siRNA from the fluorescent signal of Lysotracker™ reflects that siRNA was successfully released from the endosome, which was seen in most of the cells transfected with LNP1. This was further underlined by calculating the Pearson's correlation coefficient (PCC) (Fig. 6B), which quantified the degree of overlap between the green and red color localizations. A higher PCC value indicates a greater degree of colocalization and overlapping of these two colors.

3.5. Assessment of efficiency in submerged cell culture after storage of siRNA-loaded LNPs

Since PEG-lipids in LNP formulations are expected to facilitate colloidal stability, we evaluated this property for a period of 10 weeks. The impact of the helper lipid on the stability was also investigated. Gene knockdown efficiency of LNP formulations LNP1–4 loaded with siGFP was tested as well as siRNA loss, size and PDI over a period of 10 weeks with storage at either 4 °C or 25 °C. In general, siRNA LNPs remained stable and the siRNA intact over 10 weeks as indicated by hydrodynamic diameters below 150 nm with low PDI (Figure S 3) and high gene silencing efficiencies (Fig. 7A-D), respectively. However, minor differences started to appear across the formulations after 6 weeks (Fig. 7A-D), and they became more pronounced after 10 weeks. At this time-point, LNP1 (Fig. 7A) and LNP2 (Fig. 7B) exhibited lower gene silencing efficiency compared to LNP3 (Fig. 7C) and LNP4 (Fig. 7D), regardless of whether the samples were stored at 4 °C or room temperature. Storing the LNP formulations at room temperature led to increased loss of functionality and siRNA leakage, as indicated by siRNA loss from the LNPs (Figure S2). Conversely, LNP3 and LNP4, which contained DSPC as helper lipid, showed minimal impact from storage on their performance. Changing the PEG-lipid from PEG-DMG to PEG-DMPE did not significantly affect these properties.

3.6. Evaluation of pulmonary LNP delivery: cellular uptake and gene silencing efficiency in Calu-3 cells cultured at the ALI

To assess the suitability of the four siRNA LNP formulations for pulmonary delivery, they were tested *in vitro* utilizing Calu-3 cells cultured at the ALI. This model mimics the physiological properties of the respiratory tract more realistically, as a pseudostratified epithelium and a mucociliary differentiation can be achieved (Baldassi et al., 2022). The mucus produced by Calu-3 cells presents a significant barrier that the LNPs need to overcome to reach the cells (Kandil and Merkel, 2019; Tafech et al., 2024). To gain insight into the interaction between the LNPs and mucus, confocal images were taken of Calu-3 cells cultured at ALI and transfected with labeled siRNA-loaded LNPs (Fig. 8). The mucus produced by the cells was stained in green, the nuclei in blue, and the siRNA was labeled red. For the Calu-3 cells cultured at ALI, a homogeneously distributed thick mucus layer on top of the cells is clearly visible (Fig. 8A, B, C). Untreated cells represented blank cells (Figs. 8A). Fig. 8B shows cells treated with free, labeled siRNA as negative control. Here, the siRNA appears to be trapped within the mucus, as indicated by the red dots within the green mucus layer. This is further emphasized by the orthogonal view of the Z-stacks, where the fluorescently labeled siRNA shown in red is localized either within the green mucus layer or between the latter and the blue nuclei. Utilizing LNP2 as a delivery system for siRNA shows that some siRNA-loaded LNPs remain embedded in the mucus (Fig. 8C). However, siRNA-encapsulating LNPs were mostly present within the level of the nuclei, indicating successful cellular uptake. To accurately quantify the fluorescence levels of labeled siRNA within the cells, the cellular uptake was also assessed via flow cytometry analysis. The four LNP formulations, Lipofectamine as positive control, and free siRNA as negative control were included in the assay (Fig. 8D).

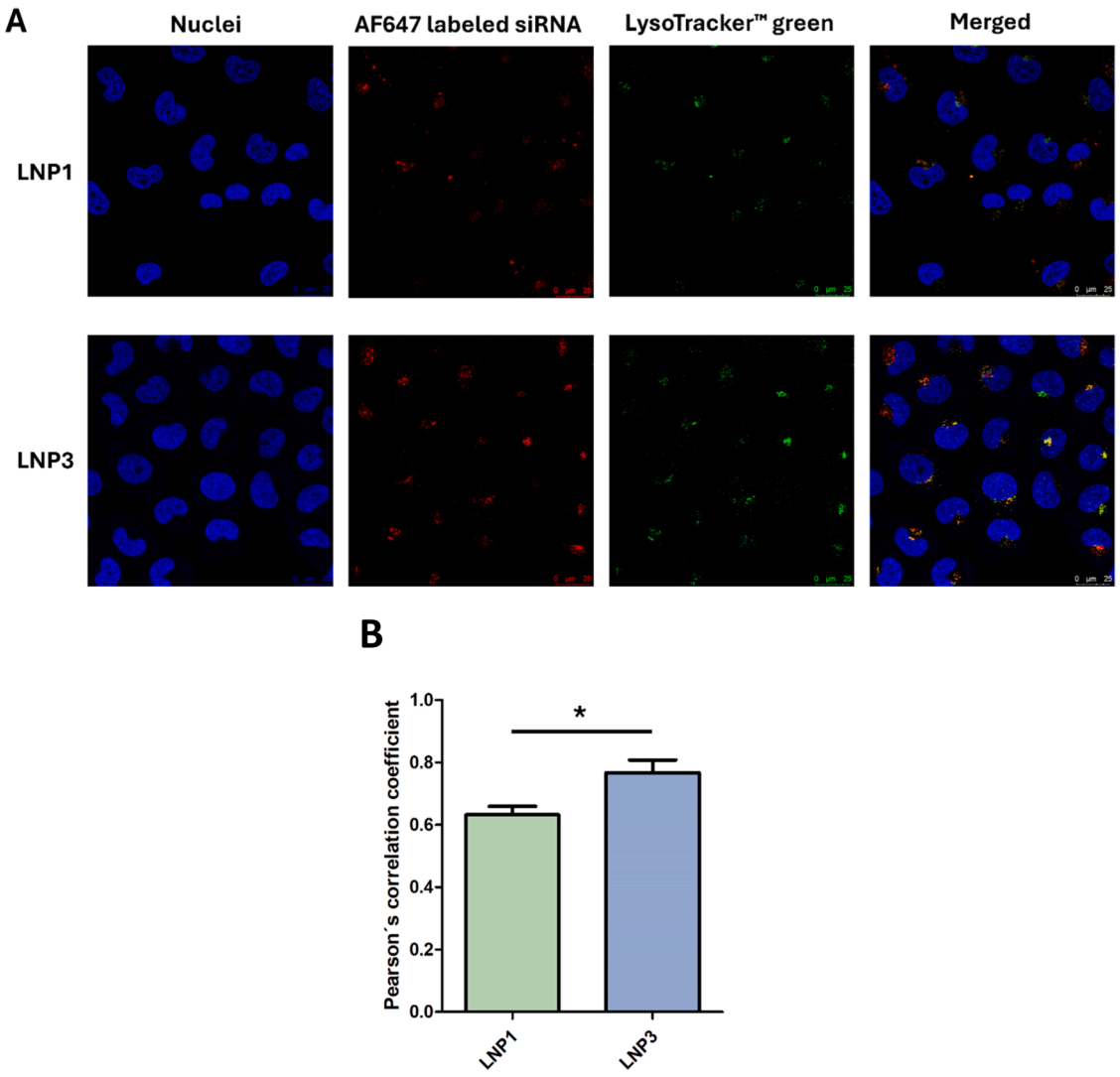

Fig. 6. Confocal imaging of endosomal escape of LNP1 and LNP3 siRNA formulations prepared via microfluidics in H1299 cells. A) H1299 cells 24 h after transfection with AF647-labeled siRNA (red) encapsulated in either LNP1 or LNP3. Nuclei stained with DAPI (blue), endosomes stained with Lysotracker™ Green. B) Pearson's correlation coefficient of the colocalization of siRNA and the endosome in H1299 cells transfected with either LNP1 or LNP3. (Values were acquired using the software ImageJ and the plugin JACoP. $n = 6$, Values are given as mean ± SEM, unpaired t-test, * $p < 0.05$).

Only LNP4 showed significant uptake. Given that positively charged lipoplexes commonly are entrapped in mucus, lipofectamine-based lipoplexes, which otherwise serve as positive control, showed no significant cellular uptake either (Sigurdsson et al., 2013). To ultimately evaluate the effectiveness of the LNP formulations for pulmonary application, a gene silencing experiment was conducted. Calu-3 cells cultured at ALI were transfected with the four LNP formulations encapsulating siRNA against GAPDH, and the Onpattro® like formulation LNP3 encapsulating siNC as control. Despite the low cellular uptake observed in Fig. 8D, all LNP formulations mediated gene silencing (Fig. 8E). Among the different lipid compositions, no significant difference in transfection efficiency was observed. However, the trend reflects that of cellular uptake, with LNP4 being the best-performing candidate.

3.7. Determination of protein corona formation on siRNA-loaded LNPs in mucus secreted by Calu-3 cells

As protein corona formation is of imminent importance for LNPs affecting their performance, including cellular uptake, immune reaction, biodistribution, and therefore targeting and transfection efficiency, we evaluated the protein corona formation on LNPs in lung cell derived mucus (Zhang et al., 2019; Debnath et al., 2023). The adsorption of proteins to the surface of various LNP formulations could elucidate the influence that different formulations have on this important process. Additionally, to better understand especially pulmonary administration, the determination of the protein corona in lung mucus is of significant interest. Regarding protein corona formation on LNPs in general, a distinction is made between two different layers of proteins on the surface of the LNP: the hard corona consisting of proteins that adsorb very strongly to the LNP surface, and the soft corona consisting of proteins that are more loosely bound due to lower binding energies (Amici et al., 2017). It is assumed that the influence of the protein corona on nanoparticles *in vivo* is almost exclusively due to the hard corona (Hartl et al., 2023). To evaluate the protein corona of LNPs incubated with Calu-3 mucus, principal component analysis (PCA) was conducted and revealed distinct clustering among LNP formulations and controls, highlighting differences in protein coronas acquired from mucus (Fig. 9A). Within the PCA, the samples are plotted based on Component 1, which differentiates samples based on the protein abundance and Component 2, differentiating samples based on the specific composition of the acquired protein corona. This enables a visualization of similarities and differences between the samples. Therefore, a clustering of

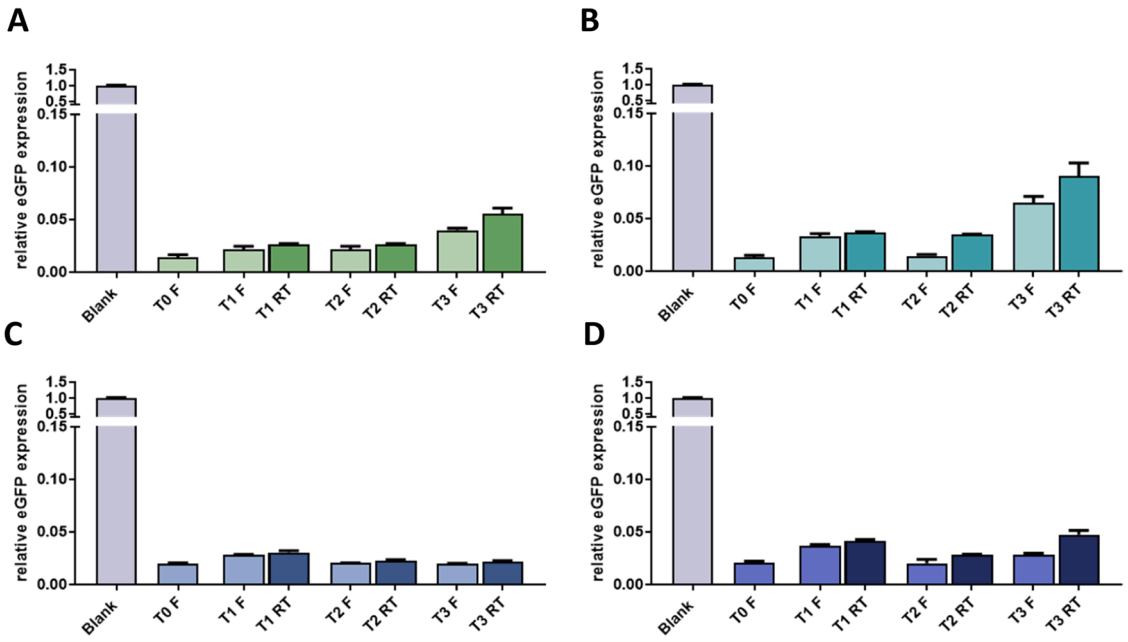

Fig. 7. eGFP gene silencing efficiencies of siRNA-loaded LNP formulations prepared via microfluidics. A) LNP1, B) LNP2, C) LNP3, and D) LNP4 in H1299/eGFP cells transfected with 100 pmol of encapsulated siGFP at different time points and after different storage conditions. T0 represents transfection with freshly prepared LNPs, T1 represents transfection results one week, T2 6 weeks and T3 10 weeks after LNP preparation. LNP formulations were stored over time at either 4 °C (samples F) or at 25 °C (samples RT). Values are given as mean ± SEM ($N = 3$).

samples indicates a shared protein corona profile. Pure mucus samples, as positive control, clustered tightly, reflecting consistent protein profiles, while the "LNP only" sample, as negative control lacking a protein corona, was distinctly separated along Component 1, which accounted for 74 % of the variance. Among LNPs, formulations LNP1 and LNP2 formed one cluster, while LNP3 and LNP4 formed another, suggesting their physicochemical properties influence protein adsorption. Component 2 (16.2 % variance) further differentiated these clusters based on specific protein corona compositions. The volcano plot (Fig. 9B) revealed that 1167 peptides were significantly and differentially associated with LNP coronas compared to mucus alone, emphasizing the complexity of LNP-mucus interactions. The left side of the volcano plot shows proteins, which are less abundant in the LNP coronas compared to the pure mucus samples, whereas the right side represents proteins, that are more abundant on the LNPs surface. Based on protein abundance, it can be concluded that LNP3 and LNP4 have larger protein coronas compared with LNP1 and LNP2 in terms of total protein quantity (Fig. 9A). This does not imply a greater diversity of protein types — rather, these formulations bind a higher overall protein amount, indicating that the bound proteins are predominantly associated with the LNP coronas compared to their presence in mucus. The high number of different proteins underscores the complexity of these interactions. The differences in protein coronas among the LNP formulations (Fig. 9C) are likely influenced by their physicochemical properties, including lipid composition, charge, and size. These variations can be expected to impact critical aspects of their behavior, such as biodistribution, clearance rates, and cellular uptake pathways (Zhang et al., 2019; Debnath et al., 2023).

4. Discussion

Comparing the physicochemical properties such as hydrodynamic diameter, zeta potential and PDI for the various LNP formulations, no striking differences were observed. Particle sizes of approximately 100 nm were obtained, which enables the LNPs to penetrate through mucus, as the micropores of lung mucus are known to be around 200 nm (Danaei et al., 2018; Kandil et al., 2023; Murgia et al., 2016; Chen et al., 2021). Furthermore, PDIs below 0.2 were achieved, displaying a desirable narrow particle size distribution (Danaei et al., 2018). Changing the formulations with regard to the helper and PEG-lipid did not significantly alter these properties of the LNPs. However, changing the RNA cargo from mRNA to siRNA had an impact on the helper lipids' encapsulation efficiency and RNA binding. While no differences were observed within the four mRNA LNP formulations, DOPE-containing siRNA formulations showed increased unbound, free siRNA compared to DSPC-containing LNPs. This could explain the higher transfection efficiencies of DOPE-containing siRNA-loaded LNPs. At first, weaker RNA binding within the LNPs seems disadvantageous. However, weaker interactions could enhance RNA release into the cytosol, leading to higher transfection efficiencies. The weaker RNA binding is also shown in the stability study, where LNP1 and LNP2 demonstrated significantly higher siRNA loss compared to DSPC-containing LNPs (Figure S 2). This siRNA leakage, along with LNP1 and LNP2 mediating less effective gene silencing after 10 weeks of storage, indicates a less stable lipid structure within the LNPs, likely due to DOPE promoting an inverted hexagonal phase compared to a lipid bilayer. An additional contributor to the reduced stability of DOPE-containing LNPs might be its heightened susceptibility to oxidation. Kamiya et al. have shown that oxidation of unsaturated lipids in mRNA-LNPs correlates with reduced transfection efficiency (Kamiya et al., 2022). As DOPE contains two double bonds, it is intrinsically more prone to oxidation than the saturated DSPC, especially under storage conditions involving oxygen, light, or elevated temperatures. Lipid oxidation can lead to structural changes, reduced encapsulation efficiency, nanoparticle and siRNA integrity, leading to impaired particle stability.

Examining gene silencing efficiency in submerged cell culture revealed significant variations among the four siRNA LNP formulations. LNP1 and LNP2 outperformed LNP3 and LNP4 despite the opposite trend for cellular uptake (Fig. 5). This discrepancy can be attributed to the use of DOPE as helper lipid instead of DSPC. Structurally, DOPE's unsaturated acyl chains and the smaller head group compared to DSPC result in a conical structure instead of the cylindrical geometry of DSPC (Fig. 1B). This enables DOPE to promote the formation of an inverted hexagonal phase (H_{II}) instead of a lamellar lipid bilayer, facilitating

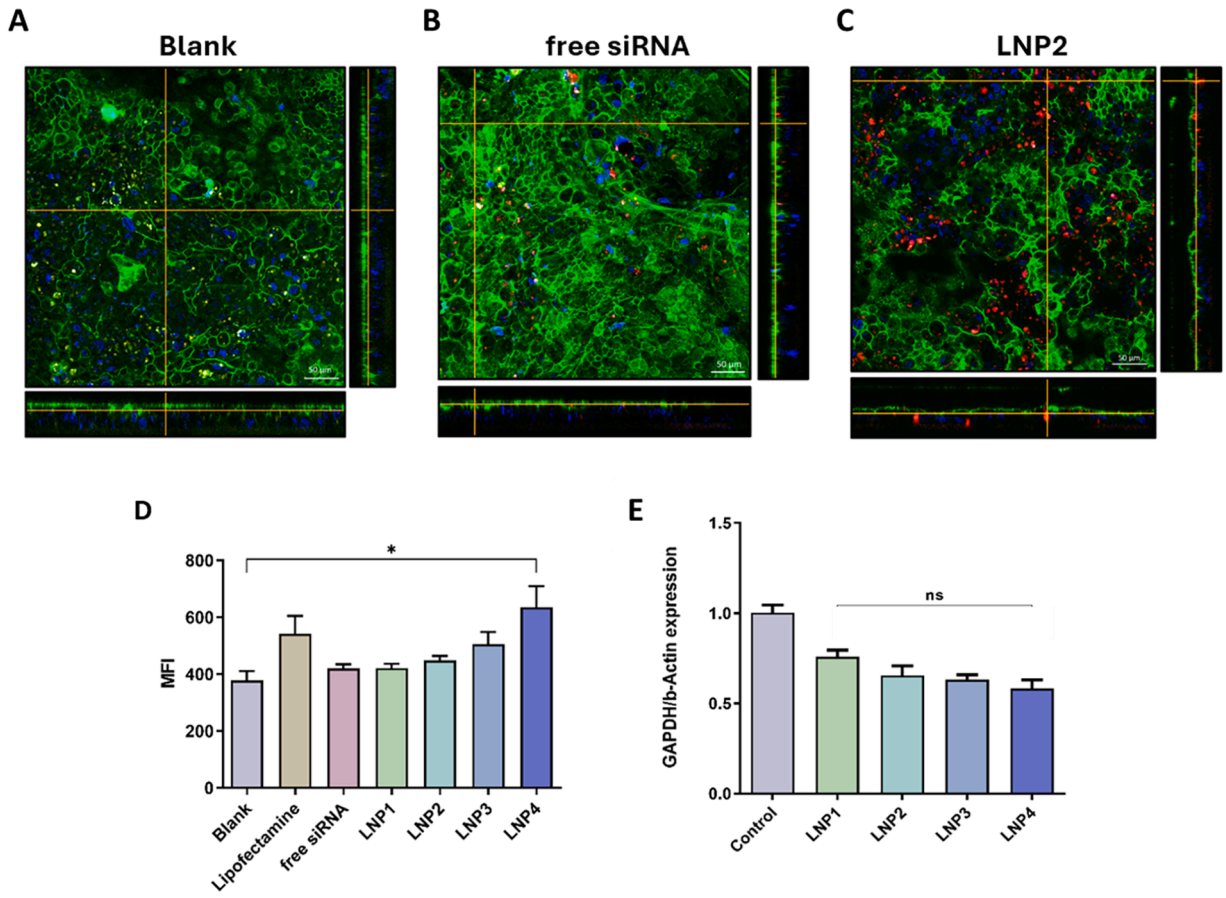

Fig. 8. Evaluation of LNP formulations LNP1–4 prepared via microfluidics regarding pulmonary delivery via ALI cell culture. Confocal images of Calu-3 cells cultured at ALI, nuclei were stained with Hoechst (blue), and the mucus layer was stained with AlexaFluor488-labeled Wheat-Germ-Agglutinin (panels A, B, C). Untreated Calu-3 cells represent blank samples (A). B) Calu-3 cells treated with 100 pmol siRNA containing 10 % Cy5-labeled siRNA C) Calu-3 cells transfected with LNP2 encapsulating 100 pmol siRNA containing 10 % Cy5-labeled RNA. D) Cellular uptake in Calu-3 cells cultured at ALI 24 h after transfection. Untreated Calu-3 cells represent blank samples. Lipofectamine encapsulating 100 pmol siRNA containing 10 % AlexaFlour488 (AF488)-labeled RNA served as positive and 100 pmol siRNA containing 10 % AF488-labeled free siRNA as negative control. Samples LNP1-LNP4 encapsulated 100 pmol siRNA containing 10 % AF488-labeled RNA. E) GAPDH knockdown in Calu-3 cells cultured at ALI. Cells were treated with 100 pmol siGAPDH encapsulated in LNP1–4 48 h prior to readout via RTqPCR, and data were normalized against β-actin. Cells treated with 100 pmol of siNC encapsulating LNP3 samples represent controls. (One-way ANOVA *, $p < 0.05$, data indicates mean ± SEM, $N = 3$).

endosomal escape. The inverted hexagonal phase is more likely to interact with and disrupt the endosomal membrane (Farhood et al., 1995). As endosomal escape is a critical bottleneck in LNPs' performance, even slight improvements can lead to higher transfection efficiencies (Suzuki and Ishihara, 2021). Hence, improved endosomal escape, shown in the confocal images, and the increased transfection efficiency of LNP1 and LNP2 is hypothesized to be caused by DOPE compared to formulations using DSPC as helper lipid. The formation of the above-mentioned inverted hexagonal phase for DOPE-containing LNPs was also shown via CryoTEM imaging (Fig. 4). We hypothesize that the appearance of discernible hexagonal structures in the LNPs at the molar ratio of 10%, which did not lead to a hexagonal phase in the study by Pattipeiluhu et al. using DOPE, may be attributed to the use of MC3 as the ionizable lipid. Pattipeiluhu et al. employed DODAP as ionizable lipid, which possesses a more cylindrical structure compared to the conical structure of MC3 (Escalona-Rayo et al., 2023). A conical structure promotes the formation of hexagonal structures, whereas a cylindrical structure favors lipid bilayers.

Interestingly, the effect of enhanced transfection efficiency was not observed in the mRNA expression experiments. This is in alignment with Kulkarni et al. where the conical structure of DOPE did not increase mRNA expression efficiency of LNPs formulated with MC3. This might be due to MC3's conical shape, which potentially facilitates endosomal escape (Kulkarni et al., 2019). Consequently, it can be assumed that the RNA cargo size and structure have a significant impact. siRNA is double-stranded and a short molecule compared to mRNA (siGFP: 21 base pairs *vs* mGFP 1,929 bases). Therefore, we hypothesize that the interaction of DOPE with the endosomal membrane creates small pores or respective disruptions that are passable for smaller siRNA molecules but not for larger and bulkier mRNA molecules. This hypothesis is supported by the endosomal escape images: LNP1 shows much higher endosomal escape compared to LNP3 where the only difference is the use of DOPE instead of DSPC. Maugeri et al. demonstrated that the endosomal escape for mRNA is <1 %, whereas Gilleron et al. reported endosomal escape of siRNA of about 2 % for comparable LNP compositions (Maugeri et al., 2019; Gilleron et al., 2013). These findings corroborate the hypothesis that larger mRNA molecules might face more challenges passing through the endosomal membrane. Overall, both hypotheses relating to RNA binding and endosomal membrane disruption suggest that siRNA release into the cytosol is increased for DOPE-containing formulations resulting in enhanced siRNA transfection efficiency. Therefore, the beneficial effects of DOPE depend on the RNA cargo, particularly when conical ionizable lipids like MC3 are used. Utilizing DOPE in these formulations significantly impacts the transfection efficiency for siRNAs or potentially other small RNA cargos.

Varying the PEG-lipid from PEG-DMPE to PEG-DMG did not notably

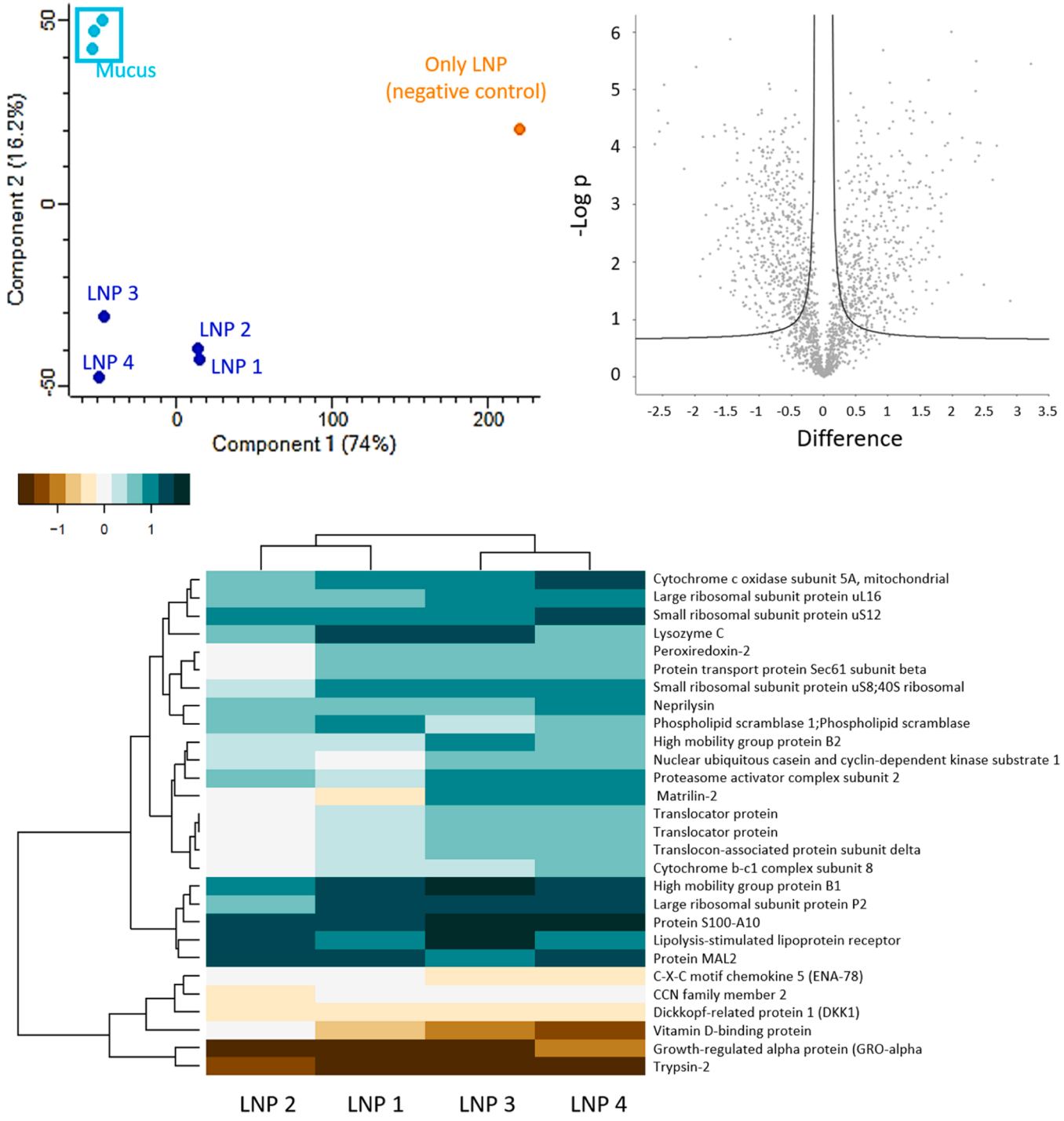

Fig. 9. Protein coronas formed on LNP formulation 1–4 prepared via microfluidics incubated with Calu-3 lung mucus. A) Principal component analysis (PCA) showing clustering patterns of protein profiles for Calu-3 lung mucus (positive control), LNP formulations 1–4 incubated with mucus, and "LNP only" samples (negative control). B) Volcano plot generated with Perseus highlighting differentially abundant proteins between mucus (positive control) and LNPs. For each protein, significance (p-value) is plotted against the log2 fold change in abundance between groups. C) Heatmap analysis of target protein abundances revealed patterns of protein enrichment or suppression across LNP formulations LNP1–4.

affect the LNP properties. These findings can be explained by the similar properties of the PEG-lipids used, which do not differ in their lipid tail anchored in the LNP. The lipid tail is considered the most important feature of PEG-lipids for LNP formulation. PEG-DMG and PEG-DMPE share the same acyl chain length of 14 C-atoms (Fig. 1A). It is expected that they do not significantly differ in shedding rate since Suzuki et al. demonstrated that the acyl length impacts PEG shedding and subsequently protein corona formation (Suzuki et al., 2020). Additionally, the molecular weight of the PEG chain is a key property of PEG lipids. As stated in the literature, PEG chains of approximately 2 kDa provide optimal surface shielding for LNPs. Shorter PEG chains ($\leq$1 kDa) offer insufficient steric hindrance and are less effective at preventing protein adsorption, while longer PEG chains ($\geq$5 kDa) impair cellular uptake and endosomal escape, thereby reducing transfection efficiency (Berger et al., 2023). Furthermore, as demonstrated by Tafech et al., PEG chain length and grafting density are critical factors for

pulmonary delivery. By altering these parameters, LNP diffusion through respiratory mucus can be significantly enhanced, thereby improving delivery efficiency to the lung epithelium (Tafech et al., 2024). Another important characteristic of LNPs is their surface charge. It can influence LNP stability, cellular uptake, and performance (Wang et al., 2023). One main difference between the discussed PEG-lipids is the negatively charged phosphate group of PEG-DMPE compared to PEG-DMG (Fig. 1A). However, as indicated by the zeta potential, the LNPs' surface charge was not altered by varying the PEG-lipid. This might be due to the effective shielding of the phosphate group by the superficial PEG chains. This shielding effect of the negatively charged phosphate group within the PEG lipid leading to near neutral surface charges was shown by Webb et al. for PEG-DSPE containing liposomes (Webb et al., 1998). This observation is likely transferable to our LNP formulations. In conclusion, the PEG-lipid exchange therefore did not have an impact on these characteristics, which is in alignment with our results. We assume that for the PEGylation of LNPs, no notable difference in physicochemical characteristics is observed as long as the same molar ratio of PEG-lipid with the same acyl and PEG-chain length, and a similar surface charge is maintained.

For pulmonary delivery of siRNA LNPs, we utilized Calu-3 cells cultured at ALI. We showed that the LNPs are capable of penetrating the mucus layer above the cells, facilitating GAPDH gene knockdown (Fig. 8E). While gene knockdown efficiency was similar across the four siRNA LNP formulations, LNP4 showed an increased cellular uptake compared to the other formulations (Fig. 8D). However, LNPs and Lipofectamine lipoplexes showed little cellular uptake in Calu-3 cells cultured at ALI, which might explain the lack of significant difference regarding gene knockdown efficiency. As the gene silencing efficiency requires initial cellular uptake in the ALI model, the challenge of LNPs reaching the cells is the first hurdle. Generally, mucus poses a significant challenge for nanoparticles administered locally to the lungs (Tafech et al., 2024). The confocal images reveal a substantial mucus layer on top of the Calu-3 cells (Fig. 8A), measuring around 25 µm thickness. This is significantly thicker than the physiological values of 7 µm for the periciliary layer and 2–5 µm for the airway surface liquid and might be a result of the cancer status of the cell line (Karamaoun et al., 2018). Despite this pathological barrier, confocal imaging and the facilitated gene knockdown suggest that LNPs can penetrate the mucus and reach the cells. This highlights the potential of therapeutic RNA-loaded LNPs for pulmonary delivery.

Previously, Zhang et al. demonstrated that exchanging the helper lipid from DSPC to DOPE impacted the plasma protein corona formation. DOPE interacted more strongly with Apolipoprotein E (ApoE) and increased hepatic accumulation compared to DSPC, which led to an increased spleen accumulation *in vivo* (Zhang et al., 2021). Given the variety of proteins present in human lung mucus, the formation of a protein corona for pulmonarily delivered LNPs is also of significant interest. In this study, we used harvested mucus from the apical side of Calu-3 cells cultured at the ALI. Sanchez-Guzman et al. identified 408 different extracellular proteins in the Calu-3 secretome. The most abundant proteins were Lipocalin-2 (lcn2), Serpina1, Serpina3, polymeric immunoglobulin receptor (pigr), Albumin, MUCA5AC (as a component of the mucus structure), and the protein kinase ssp1 (Sanchez-Guzman et al., 2021). Amici et al. showed that the *in vivo* protein corona on LNPs differs from that formed *in vitro* experiments (in plasma). They also found a greater diversity of protein species *in vivo* (Amici et al., 2017). However, for the secretome of Calu-3 cells cultured at ALI, it was shown that it does not differ notably from the secretome of primary Normal Human Bronchial Epithelial (NHBE) cells (Sanchez-Guzman et al., 2021). It is well-established that apolipoprotein E (ApoE) binding to the surface of LNPs constitutes a significant portion of their protein corona. The association of ApoE with LNPs following PEG shedding is a primary factor contributing to their enhanced hepatic uptake, as it enables LNP recognition and internalization via hepatic LDL receptors. This mechanism is deliberately exploited in Onpattro® for liver-targeted delivery (Akinc et al., 2010). For mucus penetration, our proteomics data of NPs incubated in lung mucus need to be considered, showing that the LNP surface predominantly adsorbed proteins that can physiologically interact with lipids. Among these is the lipolysis-stimulated lipoprotein receptor (LSR). We observed a significantly higher abundance of LSR bound to LNPs compared to its presence in mucus alone. LSR is a receptor protein capable of binding ApoE- and ApoB-containing lipoproteins and mediating cellular uptake. We hypothesize that while the proteomics method may not directly detect a significantly higher amount of ApoE binding to LNPs, the high abundance of LSR indirectly indicated this interaction. Furthermore, LSR could potentially facilitate cellular uptake of LNPs, complementing the known pathway via LDL receptors. Previous studies have demonstrated a stronger interaction of ApoE with DOPE-containing LNPs for intravenous administration, indicating that changes in helper lipids impact the protein corona (Zhang et al., 2021). For the mucus protein corona, our proteomics investigation revealed that LNP formulations LNP3 and LNP4 adsorbed a higher number of proteins in general compared to LNP1 and LNP2. The composition of these proteins was very similar, which we attributed to the comparable physicochemical properties such as surface charge, size, and acyl chain length of the PEG used in these formulations. It could be hypothesized that due to the formation of an inverted hexagonal phase, proteins were less likely to bind to the DOPE-containing LNPs. This configuration might decrease the accessible binding area for proteins, as many phospholipid binding proteins bind to the polar headgroup of phospholipids (Lemmon, 2008). In the inverted hexagonal phase, the headgroups of DOPE are faced inwards with their acyl chains on the outside, potentially reducing accessibility. Comparing the different LNP formulations, Annexin A2, a phospholipid binding protein, and Lysosome-associated membrane glycoprotein 2 (LAMP2) were found to be more abundant in the protein corona on LNP3 and LNP4. These two proteins play various roles in cellular processes, including endocytosis, which could potentially be linked to the increased uptake of LNP3 and LNP4 compared to LNP1 and LNP2 (Grieve et al., 2012; Leone et al., 2017).

Interestingly, we observed both trypsin-2 and antileukoproteinase bound to LNPs at significantly higher concentrations than in mucus alone. Given that antileukoproteinase binds to and inhibits trypsin-2′s protease function, we postulate that antileukoproteinase binds to the adsorbed trypsin on the LNP surface or *vice versa*. This observation, coupled with the detection of ApoE-binding LSR, suggests that the methodology may have detected both the hard and soft protein corona. These results also underscore the importance of understanding protein corona composition to improve nanoparticle design for enhanced stability, efficient cellular uptake, and precise targetability in biological systems.

5. Conclusions

This investigation of the influence of helper lipids and PEG-lipids revealed several observations. Physicochemical properties of LNPs did not differ using various lipid compositions. It also appears that substituting the PEG-lipid did not significantly alter LNP properties, if key characteristics such as the acyl chain length of the PEG-lipid and surface charge remain constant. In contrast, the conical geometry of the helper lipid DOPE positively impacted the transfection efficiency of siRNA LNPs by promoting endosomal escape through the formation of inverted hexagonal phases. This effect was not observed with mRNA LNPs, likely due to structural differences. We hypothesize that DOPE's enhanced endosomal membrane disruption may not create sufficiently large pores for mRNA, but they may be passable for smaller siRNA molecules. Thus, it is essential to consider both lipid composition and RNA cargo simultaneously. Regarding pulmonary delivery, the mucus layer on cells presents a major barrier for LNP uptake. Nevertheless, regardless of the lipid composition, LNPs achieved knockdown in human lung cancer cells cultured at the ALI, indicating their potential for

pulmonary siRNA delivery. Further optimization of lipid composition specifically for pulmonary delivery, however, could enhance the transfection efficiency of LNPs applied to the lungs. The lipid composition also affects the protein corona formed on the LNPs' surface, therefore having an impact on key properties of LNP transfection. Our results showcased the binding of many interesting lung mucus proteins to the LNP surface. The influence of these on the LNPs' fate still needs to be further investigated to understand their role in detail.

CRediT authorship contribution statement

Stina Rademacker: Writing – original draft, Visualization, Investigation, Formal analysis. **Simone Pinto Carneiro:** Writing – review & editing, Supervision, Methodology. **Müge Molbay:** Writing – review & editing, Methodology, Investigation, Formal analysis, Data curation. **Federica Catapano:** Investigation, Formal analysis. **Ignasi Forné:** Investigation. **Axel Imhof:** Resources. **Richard Wibel:** Writing – review & editing, Project administration, Funding acquisition. **Christoph Heidecke:** Project administration. **Peter Hölig:** Supervision, Funding acquisition, Conceptualization. **Olivia M. Merkel:** Writing – review & editing, Supervision, Resources, Project administration, Funding acquisition, Conceptualization.

Declaration of competing interest

Richard Wibel, Christoph Heidecke, and Peter Hölig are employees of Lipoid GmbH. Olivia Merkel is a co-founder of RNhale GmbH, scientific board member of Coriolis Pharma GmbH, AMW GmbH, and Corden Pharma International GmbH, and an advisor for PARI Pharma GmbH, Boehringer-Ingelheim International GmbH and AbbVie Deutschland GmbH on unrelated projects.

Acknowledgements

This work was supported by Lipoid GmbH and the International Graduate Program *RNAmed - Future Leaders in RNA-based Medicine* (www.rnamed.de, Elitenetzwerk Bayern / Elite Network of Bavaria). Simone Carneiro thanks the financial support from the Alexander von Humboldt Foundation. The authors thank Dr. Otto Berninghausen and Susanne Rieder from Gene Center and Department of Biochemistry Ludwig-Maximilians-Universität München for CryoTEM imaging.

Supplementary materials

Supplementary material associated with this article can be found, in the online version, at doi:10.1016/j.ejps.2025.107182.

Data availability

Data will be made available on request.

References

Akinc, A., et al., 2019. The Onpattro story and the clinical translation of nanomedicines containing nucleic acid-based drugs. Nat. Nanotechnol. 14 (12), 1084–1087.
Schoenmaker, L., et al., 2021. mRNA-lipid nanoparticle COVID-19 vaccines: structure and stability. Int. J. Pharm. 601, 120586.
Yin, H., et al., 2014. Non-viral vectors for gene-based therapy. Nat. Rev. Genet. 15 (8), 541–555.
Labaki, W.W., Han, M.K., 2020. Chronic respiratory diseases: a global view. Lancet Respir. Med. 8 (6), 531–533.
Shaffer, C., 2020. Mist begins to clear for lung delivery of RNA. Nat. Biotechnol. 38 (10), 1110–1112.
Kandil, R., Merkel, O.M., 2019. Pulmonary delivery of siRNA as a novel treatment for lung diseases. Ther. Deliv. 10 (4), 203–206.
Tafech, B., et al., 2024a. Exploring mechanisms of lipid nanoparticle-mucus interactions in healthy and cystic fibrosis conditions. Adv Heal. Mater. 13 (18), e2304525.
Hald Albertsen, C., et al., 2022. The role of lipid components in lipid nanoparticles for vaccines and gene therapy. Adv. Drug Deliv. Rev. 188, 114416.
Kulkarni, J.A., et al., 2019. On the role of helper lipids in lipid nanoparticle formulations of siRNA. Nanoscale 11 (45), 21733–21739.
Kauffman, K.J., et al., 2015. Optimization of lipid nanoparticle formulations for mRNA delivery *in vivo* with fractional factorial and definitive screening designs. Nano Lett. 15 (11), 7300–7306.
Kulkarni, J.A., et al., 2017. Design of lipid nanoparticles for *in vitro* and *in vivo* delivery of plasmid DNA. Nanomedicine 13 (4), 1377–1387.
Zhang, R., et al., 2021a. Helper lipid structure influences protein adsorption and delivery of lipid nanoparticles to spleen and liver. Biomater. Sci. 9 (4), 1449–1463.
Suzuki, T., et al., 2020. PEG shedding-rate-dependent blood clearance of PEGylated lipid nanoparticles in mice: faster PEG shedding attenuates anti-PEG IgM production. Int. J. Pharm. 588, 119792.
Knop, K., et al., 2010. Poly(ethylene glycol) in drug delivery: pros and cons as well as potential alternatives. Angew. Chem. Int. Engl. 49 (36), 6288–6308.
Baldassi, D., et al., 2022. Inhibition of SARS-CoV-2 replication in the lung with siRNA/VIPER polyplexes. J. Control Release 345, 661–674.
Carneiro, S.P., Muller, J.T., Merkel, O.M., 2024. Fluorescent techniques for RNA detection in nanoparticles. Methods Mol. Biol. 2822, 187–203.
Clogston, J.D., Patri, A.K., 2011. Zeta potential measurement. In: McNeil, S.E. (Ed.), Characterization of Nanoparticles Intended For Drug Delivery. Humana Press, Totowa, NJ, pp. 63–70. Editor.
Pattipeiluhu, R., et al., 2024. Liquid crystalline inverted lipid phases encapsulating siRNA enhance lipid nanoparticle mediated transfection. Nat. Commun. 15 (1), 1303.
Jayaraman, M., et al., 2012. Maximizing the potency of siRNA lipid nanoparticles for hepatic gene silencing *in vivo*. Angew Chem. Int. Engl. 51 (34), 8529–8533.
Escalona-Rayo, O., et al., 2023. *In vitro* and *in vivo* evaluation of clinically-approved ionizable cationic lipids shows divergent results between mRNA transfection and vaccine efficacy. Biomed. PharmacOther 165, 115065.
Suzuki, Y., Ishihara, H., 2021. Difference in the lipid nanoparticle technology employed in three approved siRNA (Patisiran) and mRNA (COVID-19 vaccine) drugs. Drug Metab. Pharmacokinet. 41, 100424.
Sigurdsson, H.H., Kirch, J., Lehr, C.-M., 2013. Mucus as a barrier to lipophilic drugs. Int. J. Pharm. 453 (1), 56–64.
Zhang, Z., et al., 2019. Brain-targeted drug delivery by manipulating protein corona functions. Nat. Commun. 10 (1), 3561.
Debnath, M., et al., 2023. Protein corona formation on lipid nanoparticles negatively affects the NLRP3 inflammasome activation. Bioconjug. Chem. 34 (10), 1766–1779.
Amici, A., et al., 2017. *In vivo* protein corona patterns of lipid nanoparticles. RSC. Adv. 7 (2), 1137–1145.
Hartl, N., et al., 2023. Protein corona investigations of polyplexes with varying hydrophobicity - from method development to *in vitro* studies. Int. J. Pharm. 643, 123257.
Danaei, M., et al., 2018. Impact of particle size and polydispersity index on the clinical applications of lipidic nanocarrier systems. Pharmaceutics 10 (2).
Kandil, R., et al., 2023. Targeted GATA3 knockdown in activated T cells via pulmonary siRNA delivery as novel therapy for allergic asthma. J. Control Release 354, 305–315.
Murgia, X., et al., 2016. Size-limited penetration of nanoparticles into porcine Respiratory mucus after aerosol deposition. Biomacromolecules 17 (4), 1536–1542.
Chen, D., et al., 2021. Enhancing nanoparticle penetration through airway mucus to improve drug delivery efficacy in the lung. Expert. Opin. Drug Deliv. 18 (5), 595–606.
Kamiya, M., et al., 2022. Stability study of mRNA-lipid nanoparticles exposed to various conditions based on the evaluation between physicochemical properties and their relation with protein expression ability. Pharmaceutics 14 (11).
Farhood, H., Serbina, N., Huang, L., 1995. The role of dioleoyl phosphatidylethanolamine in cationic liposome mediated gene transfer. Biochim. Biophys. Acta 1235 (2), 289–295.
Maugeri, M., et al., 2019. Linkage between endosomal escape of LNP-mRNA and loading into EVs for transport to other cells. Nat. Commun. 10 (1), 4333.
Gilleron, J., et al., 2013. Image-based analysis of lipid nanoparticle-mediated siRNA delivery, intracellular trafficking and endosomal escape. Nat. Biotechnol. 31 (7), 638–646.
Berger, M., et al., 2023. Effect of PEG anchor and serum on lipid nanoparticles: development of a nanoparticles tracking method. Pharmaceutics 15 (2).
Tafech, B., et al., 2024b. Exploring mechanisms of lipid nanoparticle-mucus interactions in healthy and cystic fibrosis conditions. Adv Heal. Mater. 13 (18), 2304525.
Wang, M.M., et al., 2023. Elucidation of lipid nanoparticle surface structure in mRNA vaccines. Sci. Rep. 13 (1), 16744.
Webb, M.S., et al., 1998. Comparison of different hydrophobic anchors conjugated to poly(ethylene glycol): effects on the pharmacokinetics of liposomal vincristine. Biochim. Biophys. Acta - Biomembr. 1372 (2), 272–282.
Karamaoun, C., et al., 2018. New insights into the mechanisms controlling the bronchial mucus balance. PLoS. One 13 (6), e0199319.
Sanchez-Guzman, D., et al., 2021. Long-term evolution of the epithelial cell secretome in preclinical 3D models of the human bronchial epithelium. Sci. Rep. 11 (1), 6621.
Akinc, A., et al., 2010. Targeted delivery of RNAi therapeutics with endogenous and exogenous ligand-based mechanisms. Mol. Ther. 18 (7), 1357–1364.
Zhang, R., et al., 2021b. Helper lipid structure influences protein adsorption and delivery of lipid nanoparticles to spleen and liver. Biomater. Sci. 9 (4), 1449–1463.

Lemmon, M.A., 2008. Membrane recognition by phospholipid-binding domains. Nat. Rev. Mol. Cell Biol. 9 (2), 99–111.
Grieve, A.G., Moss, S.E., Hayes, M.J., 2012. Annexin A2 at the interface of actin and membrane dynamics: a focus on its roles in endocytosis and cell polarization. Int. J. Cell Biol. 2012, 852430.
Leone, D.A., et al., 2017. Surface LAMP-2 is an endocytic receptor that diverts antigen internalized by Human dendritic cells into highly immunogenic exosomes. J. Immunol. 199 (2), 531–546.